Bull. Mater. Sci. (2022)45:36
https://doi.org/10.1007/s12034-021-02618-9

Physical properties of the semiconducting delafossite $AgNiO_2$

R BAGTACHE[1], O MAHROUA[2,*] and M TRARI[2]

[1]Laboratory of Electrochemistry-Corrosion, Metallurgy and Inorganic Chemistry, Faculty of Chemistry, USTHB, BP 32, 16111 Algiers, Algeria

[2]Laboratory of Storage and Valorization of Renewable Energies, Faculty of Chemistry, USTHB, BP 32, 16111 Algiers, Algeria

*Author for correspondence (smoussama@gmail.com)

MS received 9 June 2021; accepted 13 October 2021

Abstract. The delafossite $AgNiO_2$ was prepared by hydrothermal route. The X-ray diffraction shows a single phase indexed in a rhombohedral unit cell ($R\bar{3}m$) with a particle size of 12 nm. The Raman spectroscopy confirmed the single phase. The thermal analysis shows a stability up to 290°C. The forbidden band (0.87 eV), determined from the diffuse reflectance, is assigned to the transition: Ag^{+}: *4d* → hybridized (d_{z2}–s) – O^{2-}: 2*p* orbital. The magnetization *M*(*H*), measured at different temperatures, exhibits a low hysteresis at 200°C with a weak remanence of 495 Oe. It increases with the applied field to saturate at ∼5 kOe, suggesting a paramagnetism of $AgNiO_2$ nanocrystallites with a low spin (LS) Ni^{3+} configuration. The thermal variation of the electrical conductivity indicates a semiconducting behaviour with an activation energy (E_a) of 0.013 eV. The high conductivity (σ_{300K} = 1.8 Ω^{-1} cm^{-1}) is in conformity with the non-cooperative effect of the Jahn–Teller Ni^{3+} ion. The thermo-power shows *p*-type behaviour coming from oxygen intercalation in the layered lattice. The conduction occurs by polaron hopping between mixed valences $Ag^{2+/+}$ and increases with raising temperature, in agreement with a degenerate semiconductor. The valence band, determined from the capacitance measurements in KOH (0.1 M) electrolyte, is made up of Ag^{+}: 4*d* orbital, located at – 4.52 eV below vacuum.

Keywords. Delafossite $AgNiO_2$; hydrothermal method; semiconductor; optical properties; transport properties.

1. Introduction

The delafossites $AgMO_2$ begin to receive a growing interest in solar energy conversion and environmental protection [1–4]. Up to now, the literature reported a large number on the synthesis of delafossites with various formula such as: $AgXO_2$ (X = Al, Ga and In) [5], $CuBO_2$ (B = Al, Ga, In, B, La, Sc and Y) [6,7], $CuFeO_2$ [8], $CuMnO_2$ [9], $CuVO_2$ [10], $CuCrO_2$ [11] and $CuCoO_2$ [12]. It has also been reported that $AgNiO_2$ has a linear *s*–*p* coordination of Ag^{+} and *p*-type conduction [13–16]. Attempts to prepare Ag-delafossites by solid-state reaction have so far been unsuccessful, because of the low free enthalpy $\Delta G°$ of Ag_2O (– 11.21 kJ mol^{-1}), where silver is easily reduced at low temperatures, not exceeding 200°C. $AgNiO_2$ is a stable compound and other oxides exist in the ternary phase diagram Ag–Ni–O, like Ag_2NiO_4 and $Ag_3Ni_2O_4$. $AgNiO_2$ behaves like a semimetal, where the charge carriers are formed by a slight overlap of the band of Ag atoms with the σ* antibonding band resulting from the overlap of the Ni: 3*d*/O: 2*p* levels [16].

The delafossites offer pathways with reduced activation energy for oxygen insertion, which proceeds with a diffusion coefficient of ∼10^{-15} cm^2 s^{-1} [17] and can undergo topotactic electrochemical oxygen insertion, leading to *p*-type semiconductors [18]. Many works have been devoted to the synthesis of $AgMO_2$ (M = 3*d* element) and only the exchange reactions led to single phases [19]. So, we were motivated by chemical synthesis methods due to their photoactive properties. In our previous work, we described a facile route to prepare Ag-based compounds [20]. In continuation, we study the compound $AgNiO_2$ prepared by the hydrothermal route. We report herein the physical properties, namely, the UV-diffuse reflectance, thermal analysis, Raman spectroscopy, electrical conductivity (σ) and thermo-power (S) as well as the semiconducting characterization. The magnetic properties have also been investigated, while the electrochemical will be deferred to the next work.

2. Experimental

2.1 *Preparation of $AgNiO_2$*

Very few works were reported for the preparation of $AgNiO_2$ by hydrothermal route [21]. $AgNO_3$ (Rectapur) was dissolved

Published online: 14 February 2022

in distilled water and mixed with $Ni(NO_3)_3{\cdot}9H_2O$ (Fluka, 99%) in a molar ratio (Ag/Ni = 15 mmol/15 mmol); the mixture was transferred into a Teflon-lined stainless steel autoclave. The crystallization was realized at 200°C under autogenous pressure for 54 h to ensure a total reaction, followed by water quenching. The end product was recovered by filtration, thoroughly washed with distilled water and dried at 60°C.

2.2 *Characterization*

The phase purity was checked with a Mini-Diffractometer MD-10 using copper anticathode (λ = 0.15418 nm) in the 2θ range (20°–70°) at a step size of 0.02°. Thermal analysis (TG) was carried out on a TAG Setaram instrument at a heating rate of 10°C min^{-1} up to 750°C in air under a flow rate of 20 ml min^{-1}.

The Raman spectrum was measured by a Horiba Lab-RAMHR spectrometer laser with an excitation source direct (625 nm). The optical gap was determined with a Jasco V-650 spectrophotometer in the region 190–900 nm, attached to an integrating sphere. $BaSO_4$ was used as standard.

The Ni^{3+} concentration was indirectly determined by iodometry. An exact mass of $AgNiO_2$ (10.1 mg) was dissolved in HNO_3 (65%) in the presence of KI excess ($Ni^{3+} + I^- \rightarrow Ni^{2+} + 0.5\ I_2$); the liberated iodine was back titrated by a standard $Na_2S_2O_3$ solution. It is worthwhile to mention that Ni^{3+} must be titrated quickly to prevent its reduction into Ni^{2+} owing to its high redox potential [22].

The magnetization *vs.* applied field (*M–H*) of $AgNiO_2$ was plotted with a Vibrating Sample Magnetometer model Micro Sense EZ9 between ±20 kOe; the magnetic parameters: the saturation magnetization, coercivity and retentivity were obtained at different temperatures. The calibration at zero field was made by using $Gd_2(SO_4)_3{\cdot}8H_2O$.

$AgNiO_2$ pellets were pressed under isostatic pressure of 3 kbar and treated at 200°C, a medium density ($\sim$70%) was determined due to the low thermal stability (see below). The electrical conductivity (σ) was measured by the two-probe technique in the range 300–400 K. The thermo-power (S), i.e., the proportionality constant between the gradients of voltage (ΔV) and temperature (ΔT), was determined from the ratio (= $\Delta V/\Delta T$) using a home-built equipment; the measurements were done using a dynamical technique to produce a temperature gradient.

The working electrode was contacted by soldering a copper wire onto the back pellet with silver paint and isolated in a glass tube with hardening Araldite. The capacitance-potential (C^{-2}–E) was plotted at 10 kHz in KOH (0.1 M) electrolyte by using a PGP301 potentiostat and scaled against a saturated calomel electrode (SCE).

3. Results and discussion

The $AgNiO_2$ powder, prepared hydrothermally, exhibits a dark colour and the XRD pattern displays broad peaks, characteristic of a single phase with a nano-morphology (figure 1a). The lattice parameters, refined by the Rietveld method in the hexagonal description (figure 1b) [20]: a = 0.2930(1) nm and c = 1.8297(4) nm agree with those reported previously [ASTM 00-025-0761, PDF 4]. $AgNiO_2$ crystallizes in a rhombohedral symmetry (3R polytype, SG: $R\bar{3}m$: C_{3v}); Ni^{3+} is in a special position and occupies the centres of octahedra sharing common edges, forming infinite $_\infty[NiO_6]$ layers in the (*0 0 n*) planes, while oxygen is in a particular position with a variable coordinate z (figure 2). Ag^+ is linearly coordinated to two adjacent layers, leading to $(O–Ag–O)^{3-}$ groups parallel to the *c*-axis, with an ideal angle of 180°. This anisotropy gives $AgNiO_2$ pronounced electrical and magnetic properties in the basal planes. The Ni^{3+} ions form a triangular sub-lattice along the [001] direction in 3-sheets repeat sequence *ABC ABC*; selected interatomic distances and bond angles are summarized in table 1. The Ag–O length (0.212 nm) is slightly larger than that calculated (0.205 nm) from the Shannon ionic radii of $^{II}Ag^+$ (0.067 nm) and $^{IV}O^{2-}$ (0.138 nm) with sp^3 hybridization [23]. This indicates a low polarizability of the Ag–O bond with a certain covalency, the latter comes from the difference of electronegativity between oxygen (3.44) and silver (1.94) in the Pauling scale. By contrast, the Ni–O length (0.194 nm) is exactly equal to the sum of ionic radii of Ni^{3+} in octahedral site (= 0.056 nm, LS: $t_{2g}^6\ e_g^1$) and O^{2-}

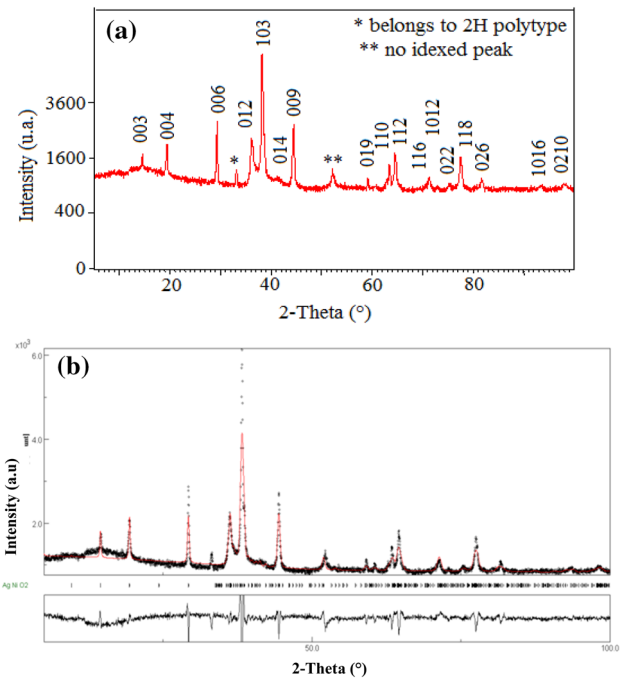

Figure 1. (**a**) X-ray diffraction pattern and (**b**) Rietveld analysis of XRD data of $AgNiO_2$ powder.

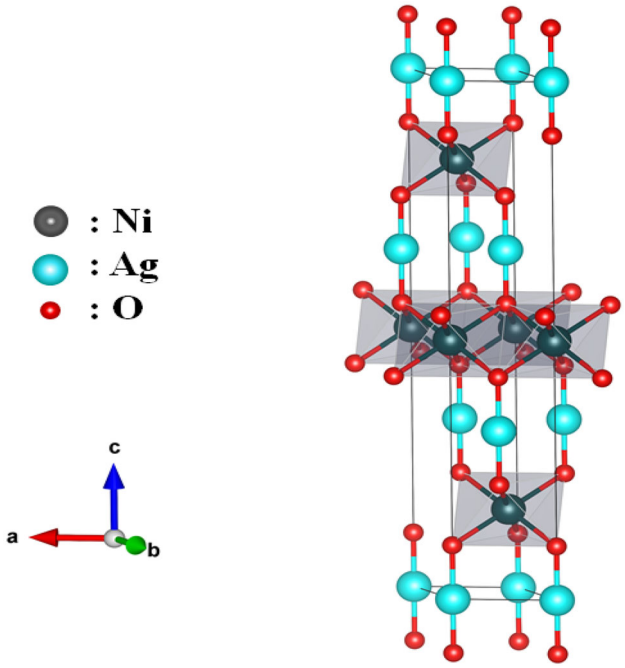

Figure 2. Projection of the structure of $AgNiO_2$ along the ac plan.

Table 1. Interatomic distances and angles of the delafossite $AgNiO_2$.

Distances (Å)		Angles (°)	
Ni–O	1.94 (5)	Ni–O–Ag	120.04 (7)
Ag–O	2.12 (6)	O–Ag–O	180.00 (0)
		O–Ni–O	97.11 (9)
		O–Ni–O	82.88 (0)

tetrahedrally coordinated (= 0.138 nm). The experimental density ($\rho_{exp.} = 7.109$ g cm^{-3}), determined by picnometry, is close to the calculated one (7.219 g cm^{-3}) {$\rho_{theo.} = Z\,M\,(N \times a^2 \times c \times \sin\gamma)^{-1}$}, where Z (= 3) is the number of formula weights per unit cell, M the molecular weight of $AgNiO_2$, a and c the lattice parameter with an angle γ of 120° and N the Avogadro number.

The mean crystallite size (D) of $AgNiO_2$ (~12 nm), evaluated from the full-width at half-maximum {FWHD = $0.94\ \lambda(\beta\ \cos\theta)^{-1}$}, indicates nanocrystallites. If we admit non-porous crystallites with spherical shapes, the minimal active surface area ($S = 6/(\rho_{exp} \times D)$) is ~70 m^2 g^{-1}.

The TG analysis of $AgNiO_2$ (figure 3) indicates a poor thermal stability; a first weight loss up to 290°C accounting for 4.02% corresponds to the decomposition (Ag + ½ Ni_2O_3), while the second loss (4.00%) is due to reduction into (Ag + NiO). Therefore, the total weight loss (8.22%) is in perfect agreement with the calculated value of 8.02%.

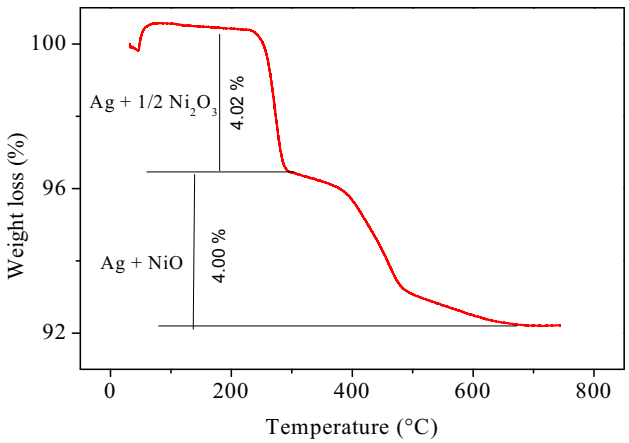

Figure 3. Thermal analysis of $AgNiO_2$ synthesized by hydrothermal route.

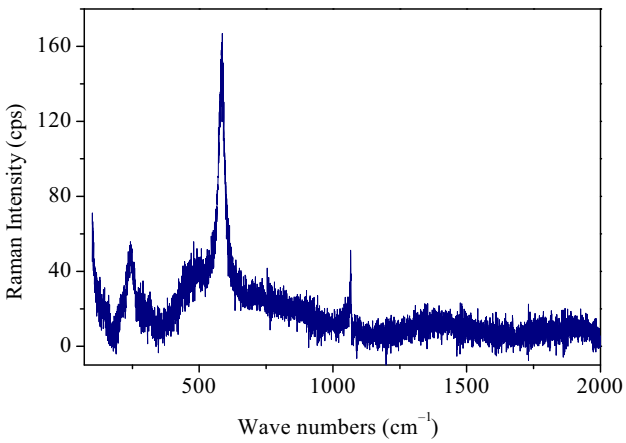

Figure 4. Raman spectrum of $AgNiO_2$.

This result explains why our attempts to prepare $AgNiO_2$ by autocombustion method (400–450°C) have failed and always gave Ag and NiO.

The mean oxidation state of nickel (3 ± 0.01), determined by iodometry, agrees with the chemical formulation. Ag^+ was titrated by potentiometry and the presence of Ag^{2+} leads to the formulation $AgNiO_{2.02}$. It should be emphasized that the degree of oxidation of Ni in $AgNiO_2$ is a problem still debated even with XAS measurements. Some authors reported a mixture of Ni^{2+} and Ni^{3+} [24], while others suggested the presence of only Ni^{3+} [13].

The Raman spectrum of $AgNiO_2$ (figure 4) shows clearly three peaks. The delafossite structure ($R\bar{3}m$) should give 12 optical phonon modes: 3 acoustic and 9 optical ($\Gamma = A_{1g} + E_g + 3A_{2u} + 3E_u$) and the phonons modes (A_{1g} and E_g) are Raman-active [25]. The movement along the hexagonal c-axis is represented by A modes, whereas the E modes correspond to vibrations in the perpendicular direction. It should be noted that there is no work on Raman spectroscopy of $AgNiO_2$.

The anisotropic structure of $AgNiO_2$ satisfies the requirement of antiferromagnetic coupling in the basal plans with a long-range order below 25 K [26]. The moments are aligned oppositely with the same magnitudes, resulting in zero susceptibility [26], the predominant interactions are negative between Ni^{3+} and the nearest neighbour via O^{2-} ions. In an octahedral environment, Ni^{3+} has ^4F spectroscopic term in the ground state with LS configuration and an effective moment of $\sim 1.7\ \mu_B$ {$= (n(n+2)^{0.5}$}. Such a point is supported by the fact that the length Ni–O (0.194 nm) is exactly equal to the sum of ionic radii {$^{IV}O^{2-} + {}^{VI}Ni^{3+}$ LS, 0.194 nm}. The variation of magnetization *vs.* applied field is measured at various temperatures (figure 5). $AgNiO_2$ shows a zero remanence and coercivity at low temperature, while a weak hysteresis appears at 200 K; this is in agreement with the supermagnetic behaviour of nanocrystalline delafossite reported by Nabiyouni *et al* [27]. The thermal contribution results in higher energy electrons causing a disruption to their order and alignment between dipoles to be destroyed, leading to a paramagnetic phase. Li *et al* reported that the crystallite size increases almost linearly with the magnetic coercivity where the nanoparticles acquire a single-domain structure. High magnetic behaviour leads to strong exchange interactions during spin alignment [28].

The relation between the absorption coefficient (α, cm^{-1}) and incident photon energy ($h\nu$, eV) is given by the formula:

$$(\alpha h\nu)^m = \text{Const} \times (h\nu - E_g) \quad (1)$$

The exponent m corresponds to the transition type: indirect (= 1/2) and direct transition (= 2). Herein, we observed only a direct transition (0.87 eV) with non-phonon assisted, occurring at Ag^+: $4d \rightarrow$ hybridized (d_{z2}–s)–O^{2-}: $2p$ orbital (figure 6).

Although the distance Ag^+–Ag^+ (0.212 nm = a-parameter) is greater than Ag (0.144 nm) [29], crystallizing in a face-centred cubic unit cell, $AgNiO_2$ exhibits a conductivity abnormally high for a delafossite. The main question to be settled is whether the charge carriers come from oxygen insertion in the layered structure or from the overlap of

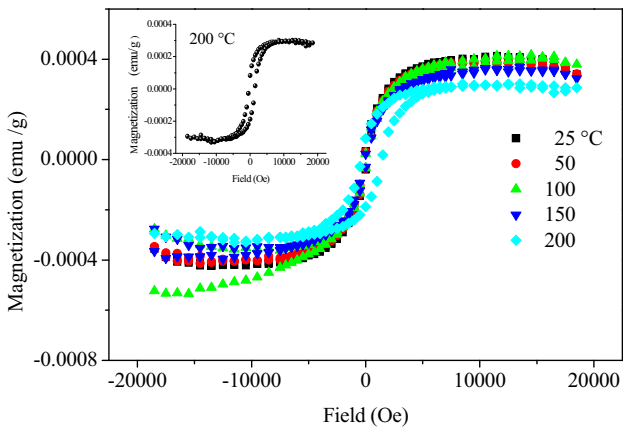

Figure 5. The magnetization-field (M–H) curve of $AgNiO_2$.

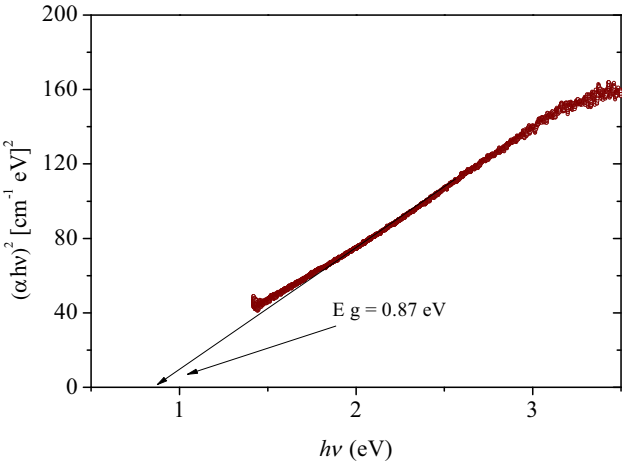

Figure 6. The direct transition of $AgNiO_2$.

Ag^+: $4d$ orbital and hybridized (d_{z2}–s)–O^{2-}: $2p$ orbital. The transport properties are somewhat controversial and a critical metal–metal distance in $3d$ oxides, above which localized electrons with semiconducting properties are expected [30]. So, the charge carriers e_g^1 should be itinerant and the holes in the NiO_6 layers are considered.

The electrical conductivity increases slightly with temperature in the region 300–400 K, (figure 7) with an activation energy (E_a = 0.013 eV), determined to form the slope dlog σ/dT^{-1}, which characterizes a degenerate semiconductor. This temperature range belongs to the thermal stability of $AgNiO_2$, which remains stable up to 290°C. In addition, the presence of a small gap implies collective electrons behaviour since no crystallographic distortion due to Jahn–Teller Ni^{3+} ion ($3d^7$) is observed unlike the monoclinic crednerite $CuMnO_2$ [31]. The delafossites are polarizable semiconductors and the electronic/ionic conduction lead to the formation of small polarons. Ag^{2+} is formed by a charge compensation mechanism where each inserted oxygen yields two Ag^{2+}, i.e., two holes with the formula

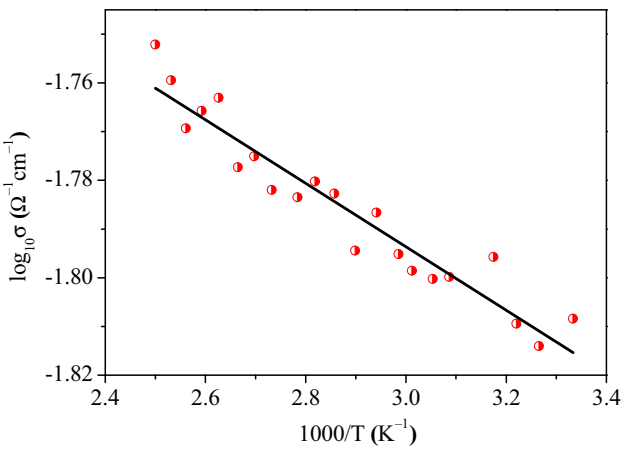

Figure 7. The logarithm of the electrical conductivity (σ) *vs.* reciprocal absolute temperature of $AgNiO_2$.

$Ag_{0.98}{}^{+}Ag_{0.02}{}^{2+}Ni^{3+}O_{2.02}$. For semi-metallic materials, the thermo-power is expressed by [32]:

$$S = \pi^2 k^2 T/3e\{d\ln\sigma/dE\}_{E=EF}. \quad (2)$$

As mentioned above, the conduction occurs in the (*a, b*) plans. The temperature dependence of the thermo-power (*S*) is shown in figure 8; the increase of *S* with *T* indicates non-interacting electrons with a hopping conduction. The small *S* value and its thermal dependence are characteristic of a degenerate conductivity with a finite density of states at the Fermi energy E_F. *S* increases from 5 to 6.5 μV K^{-1}, indicating that $AgNiO_2$ exhibits *p*-type nature with a constant carriers density (N_A) and a mobility thermally activated. The sign of *S* is correlated with that of dominant charges and suggests that the charge carriers are holes introduced by the oxygen insertion. The small *S* values (<10 μV K^{-1}) confirm the degenerate conduction, supporting the conductivity data. However, the room temperature conductivity ($\sigma_{300K} \sim 1.8\ \Omega^{-1}\ cm^{-1}$) remains too small for a classical metal.

The energies of the valence and conduction bands are determined from the capacitance measurement through the flat band potential by using the Mott Schottky relation (E_{fb}):

$$C_{SC}^{-2} = \{2/(\varepsilon\varepsilon_o eN_A)\}\{E - E_{fb} - kT/e\}, \quad (3)$$

where *A* is the electrode area, ε_o the permittivity of vacuum (8.85×10^{-12} F m^{-1}), N_A the holes density, *e* the elementary charge and *kT* the thermal energy (26 meV at ~300 K), which can be ignored. The potential E_{fb} (0.218 V_{SCE}) gives the position of the valence band (VB) and conduction band (CB) *vs.* vacuum:

$$P_{VB} = e \times E_{fb} + E_\sigma \quad (4)$$

$$P_{CB} = P_{VB} - E_g \quad (5)$$

The energies P_{VB} (–4.520 eV/+0.231 V_{SCE}) and P_{CB} (–5.390 eV/–0.639 V_{SCE}) are typical for materials whose both VB and CB derive from Ag^+: *4d* orbital and support the band scheme given elsewhere [33]. The hole mobility ($\mu_h = 2.4 \times 10^{-4}\ cm^2\ V^{-1}\ s^{-1}$), calculated from the conductivity ($\sigma = eN_A\mu_h$), is of the same order of magnitude of Ag-delafossites [20]. Such value is due to the absence of O^{2-} with no potential barrier for the electrons hopping in the Ag-plane.

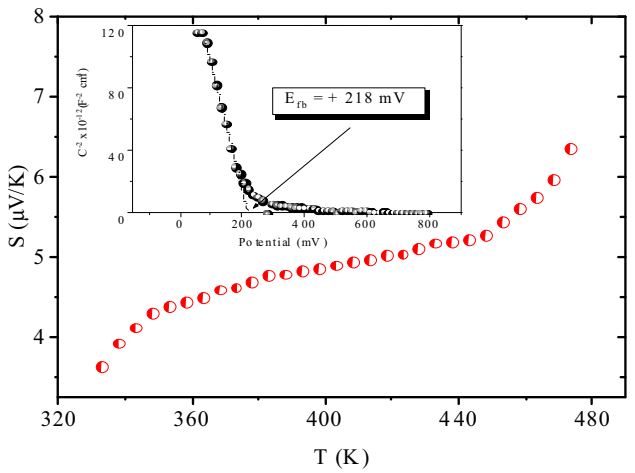

Figure 8. Thermo-power *vs.* absolute temperature and inset shows the Mott–Schottky plot at pH ~12.8 of $AgNiO_2$.

4. Conclusion

The synthesis of nanocrystallites $AgNiO_2$ by the hydrothermal method is reported for the first time and the physical properties are investigated. The oxide crystallizes in the delafossite structure and exhibits an abnormally high conductivity due to an accident structure. The direct optical gap, determined from the diffuse reflectance, corresponds to the transition: Ag^+: *4d* → hybridized (d_{z2}–s)/O^{2-}: *2p* orbital and excludes the semi-metallicity reported previously. The magnetization *M*(*H*) suggests a paramagnetism of $AgNiO_2$, while the transport properties show a behaviour similar to that of a metal with *p*-type conduction. The holes are majority carriers; originating from the oxygen insertion in the layered crystal lattice. The VB formed by Ag^+: *4d* orbital, determined from the capacitance-potential plot in KOH electrolyte, is located at –4.520 eV below vacuum.

Acknowledgements

We are grateful to Dr Abderrahmane Younès for his technical assistance in the magnetic properties and Dr Mehdi Brahim for the Rietveld analysis of the XRD. This work was financially supported by the Faculty of Chemistry (Algiers).

References

[1] Bassaid S, Chaib M, Omeiri S, Bouguelia A and Trari M 2009 *J. Photochem. Photobiol. A* **201** 62
[2] Ketir W, Bouguelia A and Trari M 2008 *J. Hazard Mater.* **158** 257
[3] El-Bassuony A A H and Abdelsalam H K 2017 *J. Alloys Compd.* **726** 1106
[4] Crespo C T 2018 *Sol. Energy* **163** 162
[5] Dong H, Li Z, Xu X, Ding Z, Wu L, Wang X *et al* 2009 *Appl. Catal. B* **89** 551
[6] Azmat Ali M, Khan A, Haider Khan S, Ouahrani T and Bin Omran S 2015 *Mater. Sci. Semicond. Process* **38** 57
[7] Koriche N, Bouguelia A, Aider A and Trari M 2005 *Int. J. Hydrog. Energy* **30** 693
[8] John M, Heuss-Abichler S, Park S H, Ullrich A, Benka G, Petersen N *et al* 2016 *J. Solid State Chem.* **233** 390
[9] Bessekhouad Y, Trari M and Doumerc J P 2003 *Int. J. Hydrog. Energy* **28** 43

[10] El Ataoui K, Doumerc J P, Ammar A, Grenier J C, Fournès L, Wattiaux A *et al* 2005 *Solid State Sci.* **7** 710
[11] Daniel U, Anamaria D, Sebarchievicia L and La Miclau M 2017 *Energy Procedia* **112** 497
[12] Beekman M, Salvador J, Shi X, Nolas G S and Yang J 2010 *J. Alloys Compd.* **489** 336
[13] Shin Y J, Doumerc J P, Dordor P, Delmas C, Pouchard M and Hagenmuller P 1993 *J. Solid State Chem.* **107** 303
[14] Wichainchai A, Dordor P, Doumerc J P, Marquestaut E, Pouchard M, Hagenmuller P *et al* 1988 *J. Solid State Chem.* **74** 126
[15] Nagarajan R, Duan N, Jayaraj M K, Li J, Vanaja K A, Yokochi A *et al* 2001 Inter. *J. Inorg. Mater.* **3** 265
[16] Sheets W C, Mugnier E, Barnabe A, Marks T J and Poeppelmeier K R 2006 *Chem. Mater.* **18** 7
[17] Sanchez R D, Torresi R M, Rettori C, Oseroff S and Fisk Z 1995 *Electrochim. Acta* **40** 209
[18] Trari M, Doumerc J P, Pouchard M, Hagenmuller P, Elazhari M, Ammar A *et al* 1994 *Ann. Chim. Fr.* **19** 521
[19] Shin Y J, Doumerc J P, Pouchard M and Hagenmuller P 1993 *Mat. Res. Bull.* **28** 159
[20] Mahroua O, Alili B, Ammari A, Ballal B, Bradai D and Trari M 2019 *Ceram. Int.* **45** 10511
[21] Sörgel T and Jansen M 2007 *J. Solid State Chem.* **180** 8
[22] Meng Y S 2012 Ph.D thesis (University of California, San Diego)
[23] Shannon R D 1976 *Acta. Crystallogr. A* **32** 751
[24] Kang J S, Lee S S, Kim G, Lee H J, Song H K, Shin Y J *et al* 2007 *Phys. Rev. B* **76** 195–122
[25] Gou G, Grinberg I, Rappe A M and Rondinelli J M 2011 *Phys. Rev. B* **84** 144101
[26] Chung J H, Lim J H, Shin Y J, Kang J S, Jaiswal-Nagar D and Kim K H 2008 *Phys. Rev. B* **78** 214
[27] Nabiyouni G, Jafari Fesharaki M, Mozafari M and Amighian J 2012 *Chin. Phys. Lett.* **27** 126401
[28] Li Q, Kartikowati C W, Horie S, Ogi T, Iwaki T and Okuyama K 2017 *Sci. Rep.* **7** 9894
[29] Hewstonand T A and Chamberland B L 1987 *J. Phys. Chem. Solid* **48** 97
[30] Weast Robert C 1997 *Handbook of chemistry and physics*, 58th edn. (Boca Raton: CRC Press)
[31] Benreguia N, Barnabé A and Trari M 2016 *Mater. Sci. Semicond. Process* **56** 14
[32] Mott N F and Davis E A 1979 *Electronic processes in non-crystalline materials* 2nd edn. (Oxford: Clarendon Press)
[33] Rogers D B, Shannon R D, Prewitt C T and Gilson J L 1971 *Inorg. Chem.* **10** 713